Characteristics of Turbulent Piloted Flames with Different Levels of Stratification

A. R. Masri*,[1], M. Juddoo[1]

[1]*School of Aerospace, Mechanical and Mechatronic Engineering,*
Faculty of Engineering and Information Technologies
The University of Sydney, NSW 2006

Stratified combustion is highly relevant in modern engines and turbines and warrants further study to resolve the effects of local concentration gradients on the flame structure. A piloted burner with two streams issuing within the pilot annulus is employed here to stabilize turbulent flames with different levels of stratification. Both inner and outer streams are flush with the burner's exit plane so that fluid with equivalence ratios, φ_i, φ_o is injected in the inner and outer streams, respectively. Compressed natural gas which is largely methane is used as fuel and the degree of stratification is defined by: $S = (\varphi_o - \varphi_i) / \langle\varphi\rangle$ where $\langle\varphi\rangle$ is the overall equivalence ratio. Stability limits are obtained for these flames at three values of $\langle\varphi\rangle$=0.6, 0.8 and 1.0. The pilot uses a stoichiometric mixture of acetylene, hydrogen and air with the same C/H ratio as methane and the burner assembly is located in a co-flowing air stream. For a given level of stratification and overall equivalence ratio, the jet velocities in both inner and outer streams are increased until the flame undergoes a transition from what looks like a Bunsen-type to that of an "open" cylindrical flame. This will be illustrated with a sequence of flames images. It is found that for a fixed overall equivalence ratio $\langle\varphi\rangle$, flame stability improves with increasing stratification but reaches an asymptote around S~1.5. High speed LIF-OH imaging is obtained at various locations in a range of flames and samples of these image sequences will be shown in the paper.

Introduction

Stratification effects are being exploited in modern engine design with the objective of maintaining overall lean-burn conditions and reducing emissions without compromising performance and responsiveness [1-5]. Typical examples include direct-injection, spark-ignited (DISI) engines where the mixtures near the spark plug are maintained rich while lean conditions prevail elsewhere in the chamber [5]. With this background, understanding the effects of different degrees of stratification on the flame structure is important and studies of stratified flames under controlled conditions are highly relevant.

Numerous experimental and numerical studies have been performed on laminar stratified flames using a range of burner geometries from counter-flow to co-flow and interested readers should consult a recent review of this topic [6]. Stratification is generally characterised in terms of the alignment between the gradient of the reaction progress variable, and that of the equivalence ratio so that maximum stratification occurs when both gradients are aligned. "Back-supported" stratification refers to the situation where excess heat and radicals from the reaction zone feeds the mixture ahead of the propagating flame front as occurs when burning occurs from stoichiometric to lean fluid. Laminar stratified, back-supported flames are found to have higher flame speeds, wider flammability limits, and more resistance to stretch than the homogeneous counterparts. The back-support is generally provided by the diffusion of heat and, in the case of rich mixtures, minor species including H_2 and CO.

Similar advances in highly turbulent stratified flames are lacking and this may be due to the difficulty of performing measurements that are sufficiently accurate to resolve the structure of such flames. Recent studies have focused on two burners: The Darmstadt burner [7,8] which is axis-symmetric and consists of three streams with the centre providing a pilot while the outer two annular channels, referred to as slot-1 and slot-2, supply mixtures at φ_1 and φ_2, respectively. The shear rate as well as the equivalence ratios φ_1 and φ_2 in the annular streams may be varied together or independently. The Cambridge burner is also axis-symmetric but with a bluff-body forming the central part of two-outer concentric streams supplying φ_1 and φ_2 [9-13]. This burner offers additional flow complexity over the Darmstadt version in the flow recirculation imposed by the central bluff-body as well as the ability to impart swirl to the outer stream. Conditions studied in both configurations cover homogeneous as well as stratified cases with values of u'/S_L up to 40 and Reynolds numbers well above 10,000 providing an extensive data set for model validation.

The present contribution explores a turbulent stratified burner that is somewhat similar to the Darmstadt configuration but with an external pilot (instead of being at the core of the non-reacting streams). Different levels of stratification are studied and the stability limits of the burner are generated for a range of overall equivalence ratios. Laser induced fluorescence imaging from the hydroxyl radical is reported for selected flames to highlight the effects of stratification on the spatial structure of the flames.

* Corresponding author: assaad.masri@sydney.edu.au

Burner and Stability Limits

A schematic of the burner is shown in Fig.1. The configuration is the same as that of Meares and Masri [14, 15] but with the inner and outer streams being flush so that two equivalence ratios, φ_i, φ_o are injected in the inner and outer streams, respectively. The two tubes within the pilot stream are the "inner" tube with an inside diameter of D_i=4mm (wall thickness of 0.25mm) and the "outer" tube with an inside diameter of D_o=7.5mm (wall thickness of 0.25mm). In this configuration, both inner and outer tubes are flush with the exit plane. The pilot shrouding the outer tube has an inside diameter of D_p =18mm and a wall thickness of 0.2mm. The burner assembly is centered in a wind tunnel with a square cross section of 15x15cm where the co-flow velocity is maintained at 15m/s throughout all current experiments.

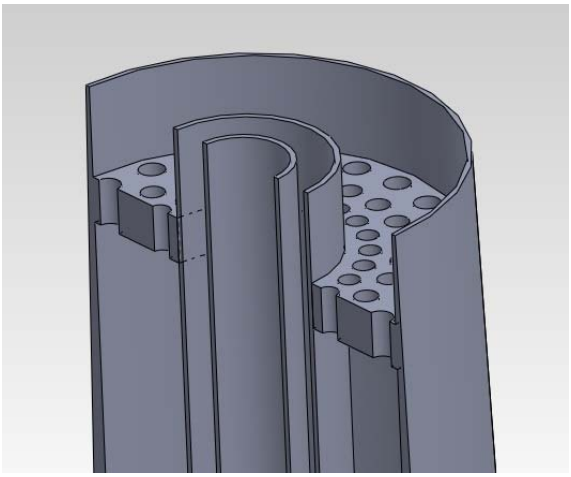

Figure 1: Schematic of the burner

The primary parameters controlling flame stability are the pilot stream, the equivalence ratios in the inner and outer streams (φ_i, φ_o) as well as the bulk jet velocities in the inner and outer streams (U_i, U_o). The fuel used here is compressed natural gas (CNG) which contains 88% CH_4, 7.8% C_2H_4, 1.9% CO_2, and 1.2% N_2 by volume with the remaining balance of 1.1% consisting of H_2, H_2O and other hydrocarbons. The pilot is maintained as a stoichiometric mixture of acetylene, hydrogen and air having the same C/H as that of methane and with an un-burnt bulk velocity, U_{pu}=1.0m/s which corresponds to a heat release rate of H_p=0.74 kW.

Figure 2 shows three sequences of photographs for a range of mixture conditions where the flames are approaching blow-off. Figure 2a (top row) shows a sequence for premixed flames with φ_i=φ_o=0.8 while sequences 2b (middle row) and 2c (bottom row) are for stratified flames such that φ_i=0.4, φ_o=1.2 for Fig. 2b (middle row) and φ_i=1.2, φ_o=0.4 for Fig. 2c (bottom row). Various images within the same sequence correspond to increasing jet velocities (both U_i, U_o) such that the same equivalence ratios are maintained. Notable in these sequences is the observation that as the jet velocity is increased, the flames approach a transition from a closed, Bunsen-shape (as shown on the far left images of Fig. 2) to one where the tip is open and only a cylindrical flame remains as shown in the far right images. The velocity at which this transition occurs is taken here to be the transition limit which is discussed next. For example, Fig. 2b (middle row) shows that the transition limit occurs in case S10-1204-130 (the naming methodology goes as follows: first 2 digits refer to equivalence ratio in the pilot which is 1.0, the next four digits refer to the equivalence ratio in the outer and inner streams φ_o=1.2 φ_i=0.4 and the last 3 digits refer to the bulk velocity in the inner stream U_i=130m/s). The visible length of the stable flames shown on the left side of Fig. 2 is about 250mm.

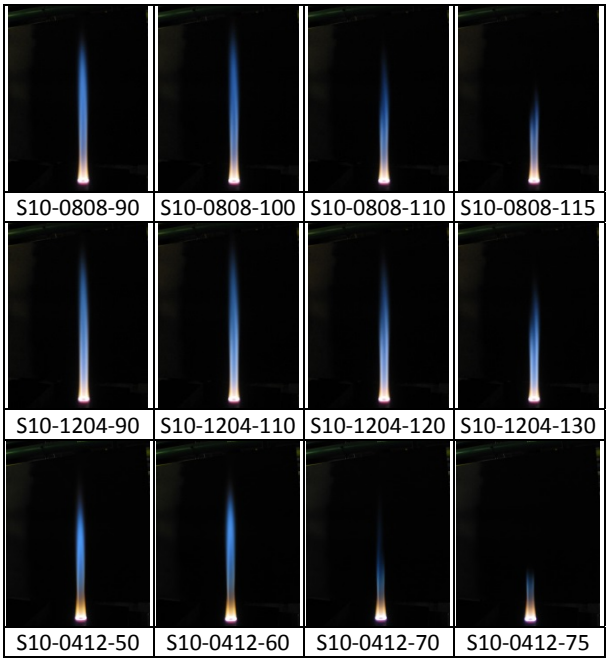

Figure 2: Images sequences for three flames with <φ>=0.8 but different levels of stratification and increasing jet velocity: (a-top row) no stratification, S=1, (b-middle row) S=1 (φ_o=1.2 φ_i=0.4), (c-bottom row) S=-1 (φ_o=1.2 φ_i=0.4),

Figure 3 shows the variation of the transition limits stratification plotted for a range of mixture strengths. The bulk velocity in the inner stream, U_i is shown on the vertical axis while the x-axis plots the extent of stratification which is given here in terms of the parameter S which is defined as:

$$S = (\varphi_o - \varphi_i, / \langle\varphi\rangle)$$

where <φ> is the overall equivalence ratio which assumes that the fluid in both inner and outer streams is well-mixed. This definition of the stratification is chosen here for convenience and other definitions based on the conditional gradient of mixture fraction may be adopted later when detailed measurements become available. Stability limits are obtained for these flames at three values of <φ>=0.6, 0.8 and 1.0. Increasing the overall strength of the mixture improves the transition limit as is expected since richer mixtures are likely to exist closer to the pilot. It is noted from Fig. 3 that as the stratification, S is increased the flame stability

improves in that the transition to an open flame is delayed but reaches an asymptote around S~1.0. With negative values of S, mixtures close to the pilot are mainly lean and hence, unlikely to induce sufficient to stabilize flames at high jet velocities. With positive values of S, there is a much higher probability of burning at the interface between the pilot and the rich mixture adjacent to it resulting in a stronger flame as is evident from the limits shown in Fig. 3. The same trends are obtained for all three cases considered here.

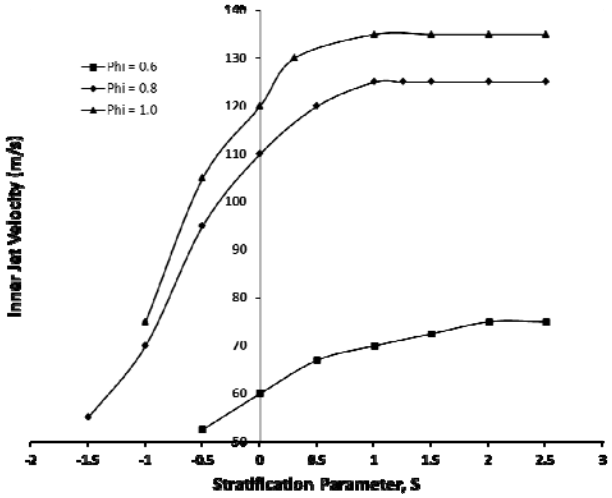

Figure 3: Transition limit, U_T from a closed to an open flame plotted with respect to the stratification parameter, S for three flames with <φ>=0.6, 0.8 and 1.0.

Table 1: Relevant parameters for the six stratified flames with of <φ>=0.8 that are selected for further measurements.

Case	S10-0808		S10-1204		S10-0412	
Strat. (S)	0	0	1	1	-1	-1
φ_i	0.8	0.8	0.4	0.4	1.2	1.2
φ_o	0.8	0.8	1.2	1.2	0.4	0.4
U_i (m/s)	79	110	90	125	50	70
U_o (m/s)	35.1	49	43.2	43.1	22.2	31.3
Re_i	20200	28000	22900	31900	5000	6900
Re_o	7850	10900	9600	13400	12700	17800
U_i / U_T	0.72	1.0	0.72	1.0	0.72	1.0
Heat (kW)	5.1	7.11	6.0	8.4	3.2	4.4

The rest of the paper focuses on flames with on overall equivalence ratio of <φ>=0.8. Six cases are selected for further measurements and properties for these are shown Table 1. It is also shown in Table 1 that three of the chosen flames are at the transition limit (U_i/U_T=1.0) while the other three have U_i/U_T=0.72. The Reynolds numbers, Re_i, Re_o are based, respectively, on the inner jet diameter and the hydraulic length of the annulus. The overall heat release is that obtained jointed from the inner and outer streams assuming complete combustion.

Imaging of LIF-OH

High-speed imaging of laser induced fluorescence from OH (HS-LIF-OH) is obtained in selected region of the three flames and at a repetition rate of 10kHz. Only representative samples of the full data set are shown here and the remaining data set may be available on request.

Imaging of LIF-OH System:

A brief description of the LIF-OH system is given here and full details may be found elsewhere [16-18]. A schematic diagram of the experimental setup is shown on Fig. 4. LIF-OH is achieved by predominantly exciting the $Q_1(6)$ line of the $A^2\Sigma \leftarrow X^2\Pi$ (1,0) system at 283.01nm. The UV beam is obtained from a SIRAH 'credo' high-speed dye laser which is pumped by an Edgewave Nd:Yag laser, with a power of 30W at 5kHz (532nm). The dye laser produces a fundamental beam at 566nm, which is then frequency-doubled to 283nm. First and second harmonics are separated from the output beam using a set of 4 Pellin-Broca prisms and the laser energy is measured to be 1.2W at 10kHz (120μJ/pulse). The beam is then expanded to a height of 50mm before being focused into a sheet (~120μm thickness) at the imaging axis.

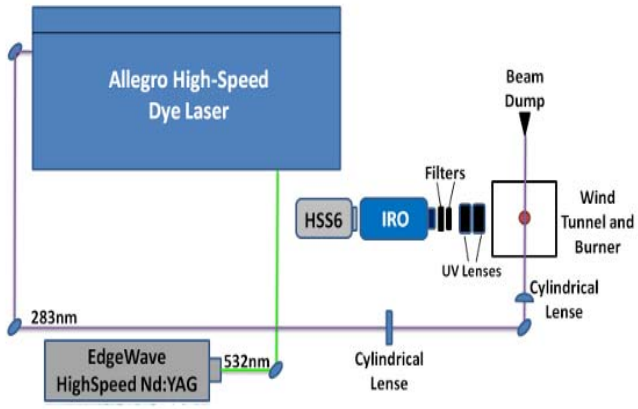

Figure 4: Experimental setup for high-speed LIF-OH imaging.

The detection system consists of a LaVision High-Speed-Star 6 (HSS6) CMOS camera with a lens-coupled, UV sensitive, two-stage intensifier (High-Speed IRO: Intensified Relay Optics, LaVision). The camera was run at a repetition rate of 10kHz with an array of 768 x 768 pixels and an image resolution of 50μm/pixel. The intensifier had a gate width of 200ns thus minimizing background luminosity. The planar

OH-LIF signal was collected using a set of LAPQ/APMQ (CVI product) three-element UV lenses, with a clear aperture of 60mm. Two filters were used, namely a UG-11 and a Semrock LP300 filter, both 1mm thick.

LIF-OH Results:

Thousands of LIF-OH images are collected for a range of axial locations in each of the flames listed in Table 1 and only a representative sample is shown in Fig. 5. The images were 50mm high and the base of each image is located at 100mm downstream of the jet exit plane. They represent, from top to bottom, the following cases: S10-1204 (for U_i=90 &125m/s), S10-0808 (for U_i=79 &110m/s), and S10-04 (for U_i=50 &70m/s) which correspond, respectively to stratification levels of 1, 0 and -1. The flames on the left side of Fig. 5 have similar departures from the transition limit with $U_i / U_T = 0.72$ which those on the right had side of Fig. 5 are right on the transition limit with $U_i / U_T = 1.0$.

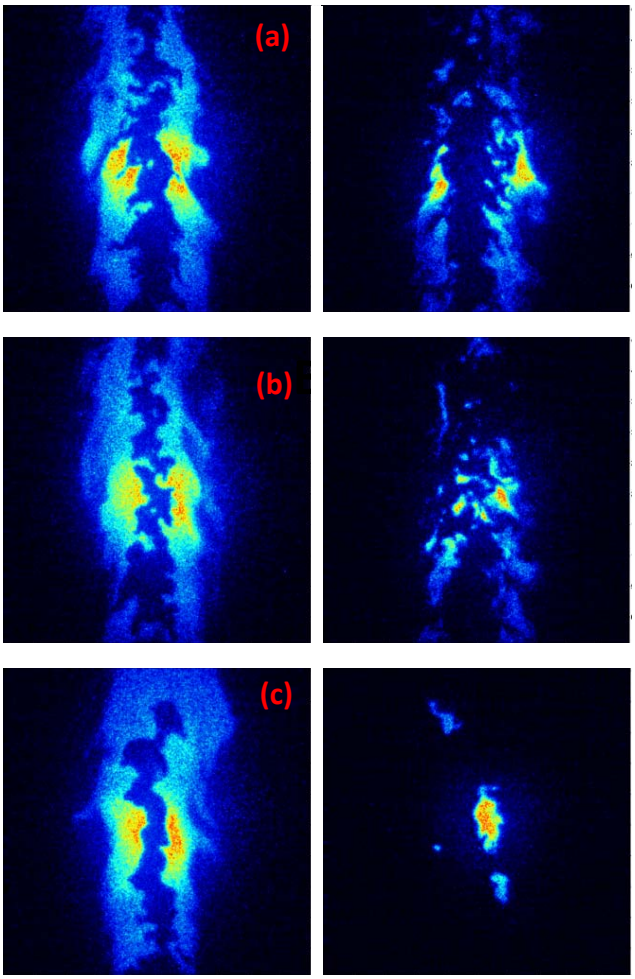

Figure 5: Sample LIF-OH images at 100mm downstream of the jet exit for cases (a) S10-1204-90(left) & S10-1204-125(right), (b) S10-0808-79(left) & S10-0808-110(right), and (c) S10-0412-50 (left) & S10-0412-70 (right). Images are 40mm wide x 50mm high.

While these images are qualitative and cannot be used to discuss absolute levels of OH, they are still useful to show the comparative spatial structure of the flames and the relative effects of stratification on parameters such as the thickness of the reaction zones. The implicit assumption here is that OH is taken as an adequate measure of the reaction zones thickness. A few observations are made:

1. Flames S10-1204-90 and S10-0808-79 show a significant degree of contortion in the reaction zone at the inner core of jet and this is consistent with the higher Reynolds number (see images on the left hand side). Flame S10-0412-50 has much less contortion since the Reynolds number is reduced by factor of about two.
2. At the transition to an open flame (plots on the right-hand side), the reaction zones become excessively fragmented with only scattered patches of OH observed for flames S10-0808-110 and S10-0412-70. The tip of these flames is gradually being broken making the transition to a cylinder-shape.
3. The reaction zone, as obtained from the OH profiles, appears to be broader for the positively stratified case (S10-1204-90) flame shown in the top row of Fig. 5.

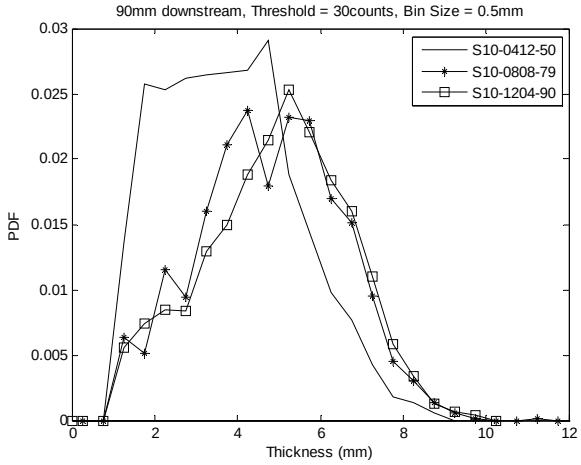

Figure 6: PDF of flame thickness as obtained from the LIF OH images collected at 90mm downstream of the jet exit plane

This is further confirmed in Fig. 6 which shows the probability density function of the OH thickness at x=90mm downstream of the jet ext plane plotted for three of the flames listed in Table 1. The results shown here use more than 1000 images and hence are statistically representative. It is evident from this plots that as the stratification changes from -1 to +1, there is increasing probability for the reaction zones to become thicker although the change from flame S10-0808-79 to S10-1204-90 is rather small but still shifted in the right direction. It could also be argued that the significant change in the thickness of OH between case S10-0412050 and the two other cases is due to the Reynolds number which is significantly lower for the former.

Further, more detailed measurements are needed to further confirm these results.

Flames with rich mixtures interfacing with the pilot stream tend to be back-supported since the reaction front propagates from rich (or stoichiometric) to leaner mixtures. This may explain why such flames are more stable and undergo a delayed transition as shown in the Fig. 3. The broader reaction zones, reflected in the OH profiles are consistent although such measurements are qualitative at best. Whether these flames show higher levels of radical species imposed by stratification effects cannot be shown here and requires more detailed measurements, similar to those reported recently by Sweeney et al. [12].

There are many other issues that may be explored with further measurements of velocity, mixing and reactive scalar fields. The extent of stratification downstream of the jet plane would be interesting. Measurements in highly inhomogenous turbulent flames show that the first five diameters are most significant in the gradual eliminations of such inhomogeneities [15]. Another issue is the transition mechanism from a closed to an open flame and the related fragmentation of the reaction zones as highlighted in the images on the right hand side of Fig. 5. The ratio of u'/S_L where S_L is the laminar flame speed is expected to higher than 10 but not sufficiently high for the flames to be in the distributed reaction zone of the regime diagram for turbulent premixed flames. Therefore, the reaction zones shown in Fig. 5 may simply be broken flamelets which dominate this transition regardless of the extent of the stratification.

Conclusions

A piloted burner is introduced here for the study of turbulent stratified flames. Stability limits improve with stratification when stoichiometric or rich mixtures are close to the pilot and leaner mixtures are on the inner stream. This is consistent with back-supported effects of stratification. Imaging of laser induced fluorescence from OH, taken as a measure of reaction zones, show slight increases in the thickness of OH profiles with increasing stratification parameter from -1 to +1. Additional, more detailed measurements are needed to further resolve the effects of stratification on the structure of these flames.

Acknowledgement

This research is generously supported by the Australian Research Council.

References

1. M.C. Drake and D.C. Haworth, Proceedings of the Combustion Institute **31 (**2007) 99-124.
2. Y. Takagi, Symposium (International) on Combustion **27 (**1998) 2055-2068.
3. Y. Yang, J.E. Dec, N. Dronniou, and M. Sjöberg, Proceedings of the Combustion Institute **33 (**2011) 3047-3055.
4. M. Yao, Z. Zheng, and H. Liu, Progress in Energy and Combustion Science **35 (**2009) 398-437.
5. F. Zhao, M.C. Lai, and D.L. Harrington, Progress in Energy and Combustion Science **25 (**1999) 437-562.
6. A.R. Masri, Proceedings of the Combustion Institute **35 (**2015) 1115-1136.
7. B. Boehm, J.H. Frank, and A. Dreizler, Proceedings of the Combustion Institute **33 (**2011) 1583-1590.
8. F. Seffrin, F. Fuest, D. Geyer, and A. Dreizler, Combustion and Flame **157 (**2010) 384-396.
9. R.S. Barlow, M.J. Dunn, M.S. Sweeney, and S. Hochgreb, Combustion and Flame **159 (**2012) 2563-2575.
10. M.S. Sweeney, S. Hochgreb, M.J. Dunn, and R.S. Barlow, Combustion and Flame **159 (**2012) 2896-2911.
11. M.S. Sweeney, S. Hochgreb, M.J. Dunn, and R.S. Barlow, Combustion and Flame **159 (**2012) 2912-2929.
12. M.S. Sweeney, S. Hochgreb, M.J. Dunn, and R.S. Barlow, Combustion and Flame **160 (**2013) 322-334.
13. R. Zhou, S. Balusamy, M.S. Sweeney, R.S. Barlow, and S. Hochgreb, Combustion and Flame **160 (**2013) 2017-2028.
14. S. Meares and A.R. Masri, Combustion and Flame **161 (**2014) 484-495.
15. S. Meares, V.N. Prasad, G. Magnotti, R.S. Barlow, and A.R. Masri, Proceedings of the Combustion Institute **35 (**2015) 1477-1484.
16. M. Juddoo, A.R. Masri, *Combustion and Flame*, 158 (2011), 902-914.
17. Meares, S., Prasad, V., Juddoo, M., Luo, K., Masri, A., Proceedings of the Combustion Institute **35 (**2015) 3813-3820.
18. V. Prasad, M. Juddoo, A. Kourmatzis, A.R. Masri, *Flow, Turbulence and Combustion,* 93, 425-437 (2014).